| Title | Control of Cross-Sections and Optical Nonlinearity of Pt Nanowires and the Roughness Effect |
|---|---|
| Author(s) | Ogata, Y.; Mizutani, G. |
| Citation | Physics Research International, 2012: Article ID 969835 |
| Issue Date | 2012 |
| Type | Journal Article |
| Text version | publisher |
| URL | http://hdl.handle.net/10119/10661 |
| Rights | Copyright © 2012 Y. Ogata and G. Mizutani. This is an open access article distributed under the Creative Commons Attribution License, which permits unrestricted use, distribution, and reproduction in any medium, provided the original work is properly cited. |
| Description | |

*Review Article*

# Control of Cross-Sections and Optical Nonlinearity of Pt Nanowires and the Roughness Effect

## Y. Ogata and G. Mizutani

*School of Materials Science, Japan Advanced Institute of Science and Technology, 1-1 Asahidai, Nomi 923-1292, Japan*

Correspondence should be addressed to Y. Ogata, ogachi.yo@gmail.com

In this paper we review our fabrication of Pt nanowire arrays on MgO(110) faceted templates by a shadow deposition method and our control of their cross-sectional shapes by adjusting the deposition directions of platinum. We obtained nanowire arrays with $C_s$ and $C_{2v}$ macroscopic symmetries. These macroscopic symmetries influence optical second harmonic generation (SHG) susceptibility elements of the nanowire arrays sensitively. On the other hand, the roughness of the nanowires had an effect on the rotational SHG patterns as a function of the sample rotation angle around the surface normal. We tried to explain the pattern change by a second-order perturbation scheme with respect to the roughness amplitude.

## 1. Introduction

Nanofabrication techniques are developing very rapidly. Analysis techniques of the produced nanostructures are also being improved year by year. Nanostructures are characterized by several parameters. Among them, symmetry parameters are important. The symmetry of the nanostructures should have an influence on their dielectric property through the electronic and vibrational wave functions in their constituting atoms and bondings. Second-order nonlinear optical phenomena are forbidden for centrosymmetric structured materials. Hence, the second-order nonlinear optical process should be sensitive to the symmetry of nanostructure shapes.

Optical second harmonic generation (SHG) is a coherent nonlinear optical process and its efficiency depends not only upon the electronic properties but also upon the symmetry of the geometrical structure of the medium [1–3]. SHG does not occur in centrosymmetric bulk media [4]. Thus, if we fabricate nanowires with broken symmetry, new optical properties should be induced in their nonlinear optical susceptibility $\chi^{(2)}$. Metallic nanowires have been known to show unique optical properties due to their strong anisotropy and electronic confinement. Also in the long run, using the nonlinear optical properties of the metallic nanowires,

powerful applications to optical devices such as frequency converters are expected [5].

Schider et al. investigated linear optical properties of metallic nanowires prepared by electron beam lithography systematically [6]. They found that the optical response of the noble metal nanowires depended strongly on the polarization of the light field. Plasmon excitation was judged to induce the enhancement of the local electric field intensity.

SHG is one of the lowest-order nonlinear optical effects. Research of the polarization dependence of SHG from the ZnSe nanowires grown on Si substrate using vapor-liquid-solid method was reported [7]. The observed SHG intensity dependence on the polarization angle may offer a development of polarization-sensitive nonlinear optical materials. SHG properties of Au and Pd nanoparticles and Au connected nanoparticles were also studied [8–10]. They analyzed the observed enhancement of the SHG intensity by using RCWM (rigorous coupled wave method). They found that the SHG intensity was enhanced due to the missing particles in the array. SHG from metal nanocylinders was also investigated in detail by using numerical electromagnetic simulation of the electric quadruple excitation [11]. They discussed the local field enhancement by surface plasmon polariton modes in the metallic nanorods. However, so far as we
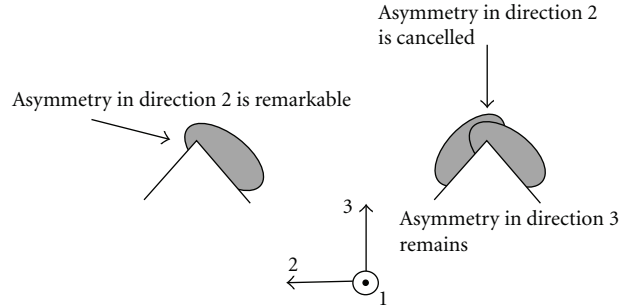
FIGURE 1: Schematic cross-sectional shapes of Pt nanowires on MgO(110) substrate fabricated in this study. (a) Pt nanowires are on one face of the facet but are seen to extend beyond the top of the facet. The edge of this extending part has more sharp curvature. (b) Pt nanowires on the two faces of the facet are connected at the top of the facet and its cross-section shape becomes symmetric with respect to the substrate normal.

know, rare attention has been paid to the correlation between the cross-sectional shapes of the nanowires and their SHG response.

We fabricated metallic nanowires on faceted NaCl or MgO(110) templates by a shadow deposition method [12–15]. The shadow deposition method for forming a periodic metal nanowire arrays uses a self-shade effect by macrostep structures on a substrate face. It was first used for submicron nanowires [16] and then was developed for wires of several tens of nanometers widths by Sugawara and Mae [17]. When a NaCl or MgO(110) substrate surface is annealed in vacuum, the surface becomes faceted with (100) and (010) planes in order to minimize its surface energy. The atomic beam from an effusion cell irradiates the faceted template, and the metal is deposited on the slopes facing the atomic beam. In this method, the nanowire arrays can be obtained at once. The magnetic properties of Fe nanowires fabricated in this way were found to be dominated by a strong in-plane shape anisotropy [18]. One big advantage of this shadow deposition method is that the fabricated nanowire arrays have macroscopic sizes as big as 10 mm × 10 mm.

Kitahara et al. obtained samples of Au nanowire arrays sandwiched by SiO layers for the TEM observation by a lift-off method, utilizing a water solubility of NaCl substrate [12]. However, the preparation of the cross-sectional samples was not easy since the cooling liquid used during cutting contains water and the NaCl substrate cannot support the wire arrays. Hence, we used MgO as the substrate forming a facet template. MgO does not solve in water and it can support the nanowire array during and after the cutting. Thus, we can prepare a cross-sectional sample cut perpendicular to the nanowire axes with MgO template substrates.

In this paper, we discuss two types of broken symmetry fabricated in the Pt nanowires through shadow deposition method on the MgO substrate. In the left cartoon in Figure 1 Pt nanowires are found to be formed on one side of the facets. The cross-sectional shapes of the nanowires were like a tilted ellipse, but parts of the Pt are seen to extend beyond the tops of the facets. A part of platinum covering the top has a thin sharp structure, and the symmetry of their cross-sectional shape is broken greatly in horizontal direction as well as in

the normal direction. The existence of such sharp wire parts of platinum of width 1 to 2 nm predicted that it is possible to fabricate Pt nanowires of 2 nm width. In fact in a separate experiment we succeeded in fabricating a 2 nm width Pt nanowire array by using a MgO(210) facet template [19].

Next, we see the right cartoon in Figure 1. Platinum was evaporated from two different directions onto the faceted template. The Pt nanowires on the two faces of the facets are connected at the top of the faceted template. Its cross-section become symmetric with respect to the substrate normal [20]. The cross-sectional shape looks like a boomerang. The cross-sectional shapes still have asymmetry in the direction normal to the MgO substrate.

Here we focus on the relation between the cross-sectional shapes and the nonlinear optical response of the two kinds of the fabricated nanowires. In order to examine the sensitivity of the nonlinear optical properties to the difference of cross-sectional shapes, we focus our attention on the nonlinear susceptibility $\chi^{(2)}$. The SHG intensity is proportional to the square of the absolute value of $\chi^{(2)}$. If the nonlinear susceptibility $\chi^{(2)}$ can be controlled, development of new optical nonlinear materials will be promoted. In this study, we detect the change of nonlinear susceptibility element $\chi^{(2)}_{ijk}$ by the difference of the symmetry of Pt nanowire cross-sectional shape.

There is one important geometrical parameter leading to rather unfavorable consequences in nonlinear optical properties. It is the roughness in the nanowire structures. The roughness generally lowers the symmetry of nanostructures, induces relaxation in the dielectric response, and generates local disturbance in the exciting electric field. Hence, it is also crucial to discuss the effect of the roughness and its control when fabricating metallic nanostructures.

In our study, roughness occurred in the fabricated nanowires due to the characteristic of our sample preparation method. Due to this roughness, the experimental SHG patterns of the boomerang cross-sectioned nanowires could not be reproduced completely in a phenomenological analysis assuming ideal $C_{2v}$ symmetry. Therefore, we analyzed the contribution of the roughness to the SHG response of Pt nanowires.
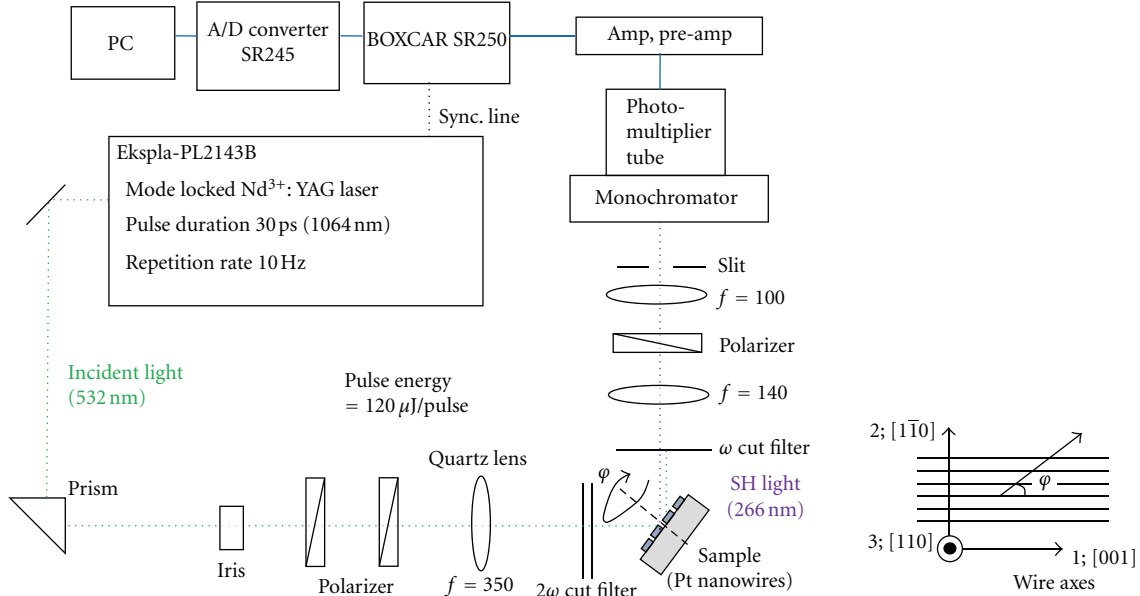
Figure 2: Block diagram of the SHG experimental setup.

## 2. Experimental

MgO(110) faceted surfaces were fabricated through a homo-epitaxial growth process using electron beam deposition. The MgO substrate surfaces became faceted by self-organization with the periodicity depending on the homo-epitaxial growth [14, 15, 20]. The facet formation of the surface was confirmed by reflection high-energy electron diffraction. Both Pt nanowires with the elliptic and boomerang-like cross-sectional shapes on the faceted MgO(110) templates were fabricated by the shadow deposition technique in a UHV chamber with base pressure of $9.5 \times 10^{-7}$ Pa. For the nanowires of elliptic cross-sections, the platinum of 4 nm nominal thickness was evaporated at room temperature from one direction with an incident angle of 65° from the faceted MgO template normal. Here the nominal thickness means the one monitored by a quartz thickness monitor with its sensor plate set perpendicular to the beam direction. For the nanowires of boomerang cross-sections, the platinum of 2 nm nominal thickness was deposited at room temperature from two directions with an incident angle of 70° from the faceted MgO template normal. After the deposition, the arrays of Pt nanowires on the templates were protected by depositing SiO of 5 nm thickness from the normal direction.

The cross-section samples for the TEM observation were fabricated by an ion milling method. Pt nanowires on the MgO(110) faceted template were first protected by epoxy resin. After solidification, wires were cut toward (001) in $400\,\mu m$ thickness. Next, the sample was set on a single hole grid and was ground to $50\,\mu m$ thickness by using a dimple grinder. The (001) flake of the MgO substrate was further ground to $2$–$4\,\mu m$ thickness by using Precision Ion Polishing System (GATAN/PIPS) equipped with argon ion beam at 3 keV. The obtained thin MgO (001) flake with Pt nanowires

was observed from [001] direction by a transmission electron microscope (TEM: H-9000NAR, Hitachi Co. Ltd).

Figure 2 shows the experimental setup for SHG measurements schematically. For measuring the SHG intensity from the Pt nanowire array, we used a frequency-doubled mode-locked $Nd^{3+}$: YAG laser with pulse duration of 30 ps, repetition rate of 10 Hz, and photon energy of 2.33 eV. We used a pulsed laser with 30 ps pulse duration because it has much bigger peak power than continuous or nanosecond lasers and it lets us observe SHG from the nanowire samples more easily. We tuned the laser carefully because the SHG intensity depends remarkably on the time profile of the output pulses determined by the condition of the laser. The maximum pulse energy was around 0.12 mJ per pulse or 1.2 mW in average, and the pulses were off-focus on the sample with 2 mm $\varphi$ diameter. In this condition the thermal effect and the damage to the sample can be regarded as negligible. The pulse interval 0.1 sec was so long that the phenomenon in each pulse does not affect the one in the next pulse. Therefore, SHG does not strongly depend on the pulse frequency. The incident light was passed through a $2\omega$ cut filter and a polarizer and irradiated the sample at the incidence angle of 45°. The input laser beam was sufficiently off-focus and the wire arrays were quite uniform in the sample area of 10 mm × 10 mm. Thus the inhomogeneity in the spatial intensity distribution of the input beam did not influence the integrated SHG intensity. In order to measure the azimuthal angle dependence of the SHG intensity, the sample was mounted on a rotation stage. The reflected SHG light beam was passed through lenses, a polarizer, an $\omega$ cut filter and a double-monochromator and was detected by a photo-multiplier.

Figure 3 shows the configuration of the polarization and azimuthal angle dependence of SHG intensity measurement

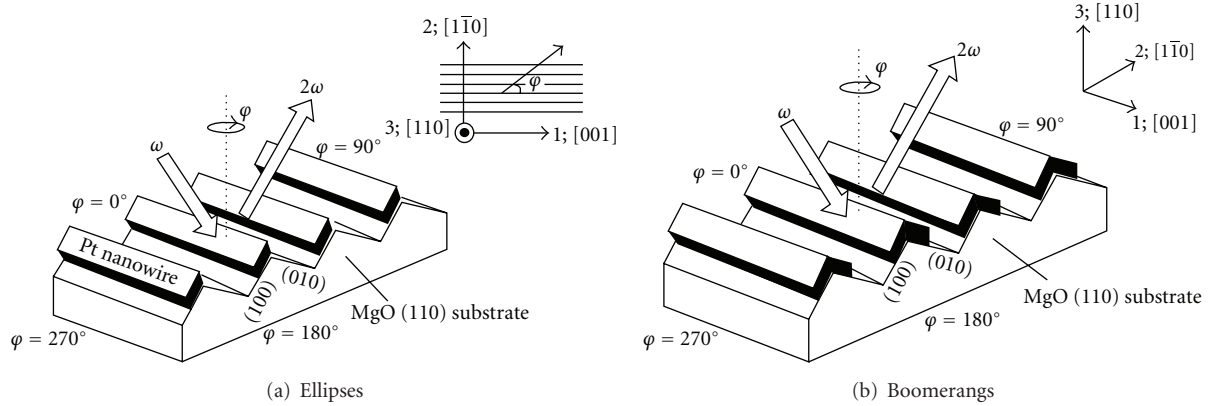(a) Ellipses                                                     (b) Boomerangs

Figure 3: Configuration of the Pt nanowires with (a) elliptic and (b) boomerang-like cross-sectioned shapes in the SHG intensity measurement. The sample rotation angle $\varphi$ is defined as the angle between the incident plane and the wire axes as shown in the center. The incident light is defined to travel in the same direction as the atomic beam during the deposition when $\varphi = 270°$.

from the two Pt nanowire arrays. The SHG intensity was measured as a function of the sample rotation angle $\varphi$. The rotation angle $\varphi$ is defined as the angle between the incident plane and the wire axes oriented in the [001] direction of the MgO substrate. When $\varphi$ is set at 270°, the incident light is defined to travel in the same direction as the Pt atomic beam during the Pt deposition.

## 3. Results and Discussion

*3.1. Transmission Electron Microscope Images of the Pt Nanowires.* Figures 4(a) and 4(b) show the plan-view transmission electron microscope (TEM) images. Well-aligned two kinds of Pt nanowires run along [001] direction on the MgO(110) substrate. The average width of both nanowires was ~7 nm. The minimum and maximum widths of the Pt nanowires with elliptic and boomerang-like cross-sections were 2.3 and 10.0 nm, and 1.3 and 13.8 nm, respectively, as seen in Figure 4(c). In Figure 4(b) we find a lot of imperfections of the nanowires than those seen in Figure 4(a). Later in this paper one will find that these imperfections influence the SHG response of the Pt nanowires.

Figure 5 shows the cross-sectional TEM images of the fabricated Pt nanowires on the MgO(110) substrate. In Figures 5(a) and 5(b), the shape of platinum on the faceted MgO substrate was like tilted ellipses and boomerangs, respectively. In the TEM image in Figure 5(a), the platinum is seen to extend beyond the tops of the MgO facets. In the expanded TEM image in Figure 4(a), thin Pt bands are seen at 91% of the left-hand side edges of the nanowires. The structure of the elliptic nanowires in Figure 5(a) is $C_s$ symmetry with a mirror plane in 2-3 direction. The structure of the boomerang nanowire in Figure 5(b) is $C_{2v}$ symmetry with mirror planes both in the 1–3 and 2-3 directions. Here, 1, 2, and 3 indicate the [001], [1$\bar{1}$0], and [110] directions of the MgO substrate, respectively.

*3.2. Optical Second Harmonic Generation from the Nanowire Arrays.* The SHG signal is generated from several nm thickness in the sample. Thus the conversion efficiency of the

fundamental into SHG photons is very low and it is around $10^{-13}$. In this case, higher-order effects will be much weaker than SHG and are not observable. In addition, the third-order nonlinear optical effect like third harmonic generation (THG) gives quite different output wavelength so that the signal was blocked by the monochromator and was not detected.

Figure 6 shows the angular SHG intensity pattern as a function of the sample rotation angle $\varphi$ around the substrate normal. The SHG intensity pattern is strongly dependent upon the rotation angle $\varphi$ and shows anisotropic shape for all polarization configurations.

We reproduce the SHG intensity patterns from Pt nanowires with elliptic cross-sections in Figures 6(a)–6(d). The SHG pattern in the $p$-in/$p$-out polarization configuration in Figure 6(a) shows two unequal lobes at $\varphi = 90°$ and 270°. The one in the $p$-in/$s$-out polarization configuration in Figure 6(b) shows two small lobes at $\varphi = 0°$ and 180°. The one in the $s$-in/$p$-out polarization configuration in Figure 6(c) shows one main lobe at $\varphi = 270°$. The one in the $s$-in/$s$-out polarization configuration in Figure 6(d) shows two lobes at $\varphi = 0°$ and 180°. This SHG intensity pattern has macroscopic $C_s$ symmetry. It is consistent with the microscopic symmetry of the nanowires.

Likewise, we reproduce the SHG intensity patterns from Pt nanowires with boomerang cross-section in Figures 6(e)–6(h). The pattern in the $p$-in/$p$-out polarization configuration in Figure 6(e) shows two equal lobes at $\varphi = 90°$ and 270°. The one in the $p$-in/$s$-out polarization configuration in Figure 6(f) shows nearly isotropic response but has four dim maxima at $\varphi = 45°$, 135°, 225°, and 315°. The one in the $s$-in/$p$-out polarization configuration in Figure 6(g) is isotropic. The one in the $s$-in/$s$-out polarization configuration in Figure 6(h) is elliptical with maxima at $\varphi = 0°$ and 180°. All the patterns in Figures 6(e) to 6(h) are symmetric with respect to the 0°–180° axis line. Thus the SHG intensity patterns have macroscopic $C_{2v}$ symmetry. It is consistent with the microscopic symmetry of the nanowires.

The SHG intensity patterns in Figure 6 have been analyzed phenomenologically using a least-squares fitting
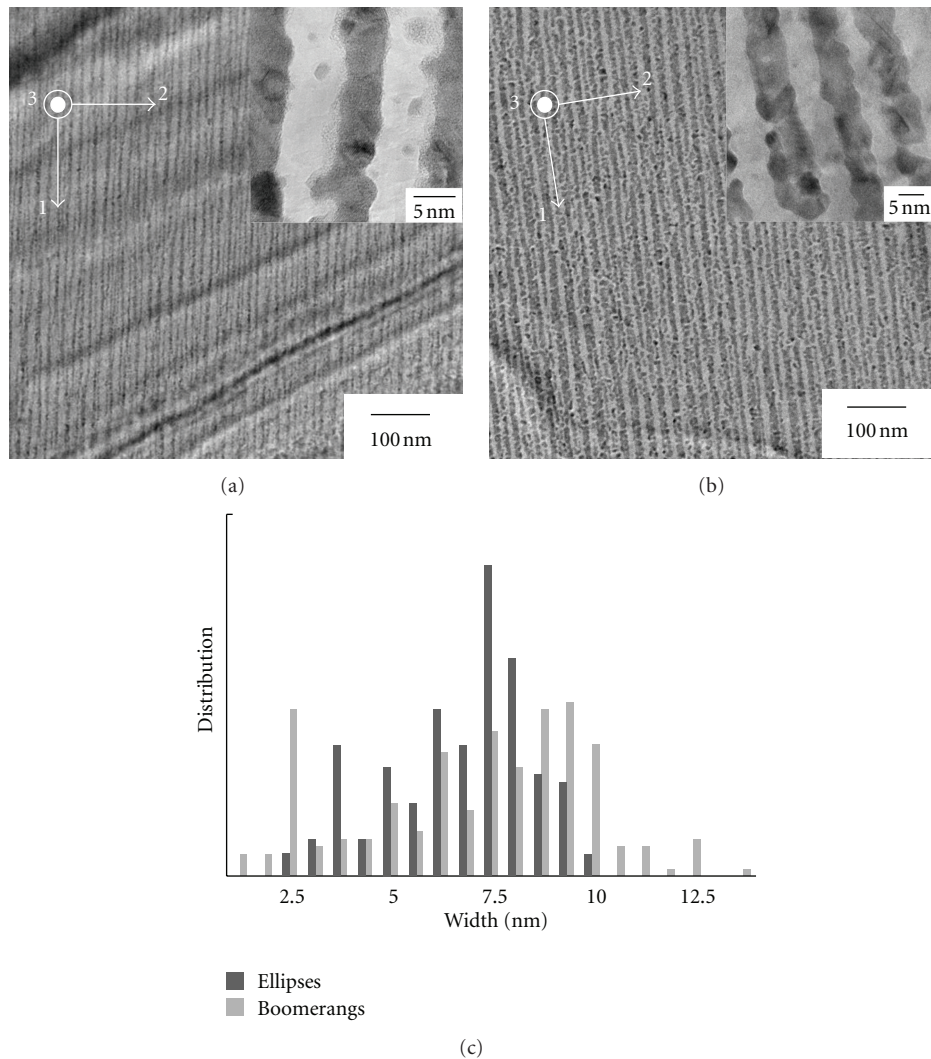
(a)

(b)



(c)

FIGURE 4: Pt nanowires with (a) elliptic and (b) boomerang cross-sections observed by TEM and their expanded images (inset). (c) Distribution of nanowire widths in the two types of nanowire arrays.
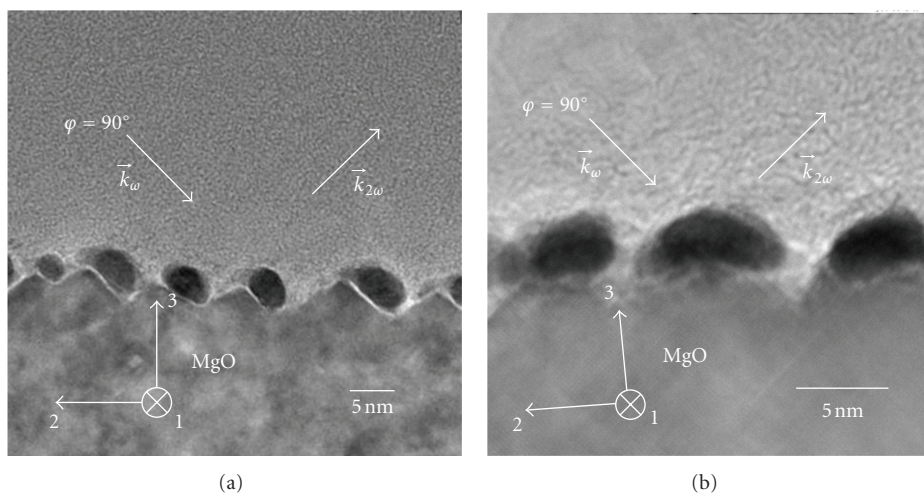


(a)

(b)

FIGURE 5: The cross-sectional TEM images of Pt nanowires showing (a) elliptic and (b) symmetric boomerang shapes on the MgO(110) faceted substrates. The MgO substrate is seen in the lower part of each panel. Two arrows indicate the wave vectors, $\mathbf{k}_\omega$ and $\mathbf{k}_{2\omega}$, of the incident and SHG light beams for $\varphi = 90°$, respectively.

*p*-in/*p*-out

$\varphi = 90°$

(a)

*p*-in/*s*-out

(b)

*s*-in/*p*-out

(c)

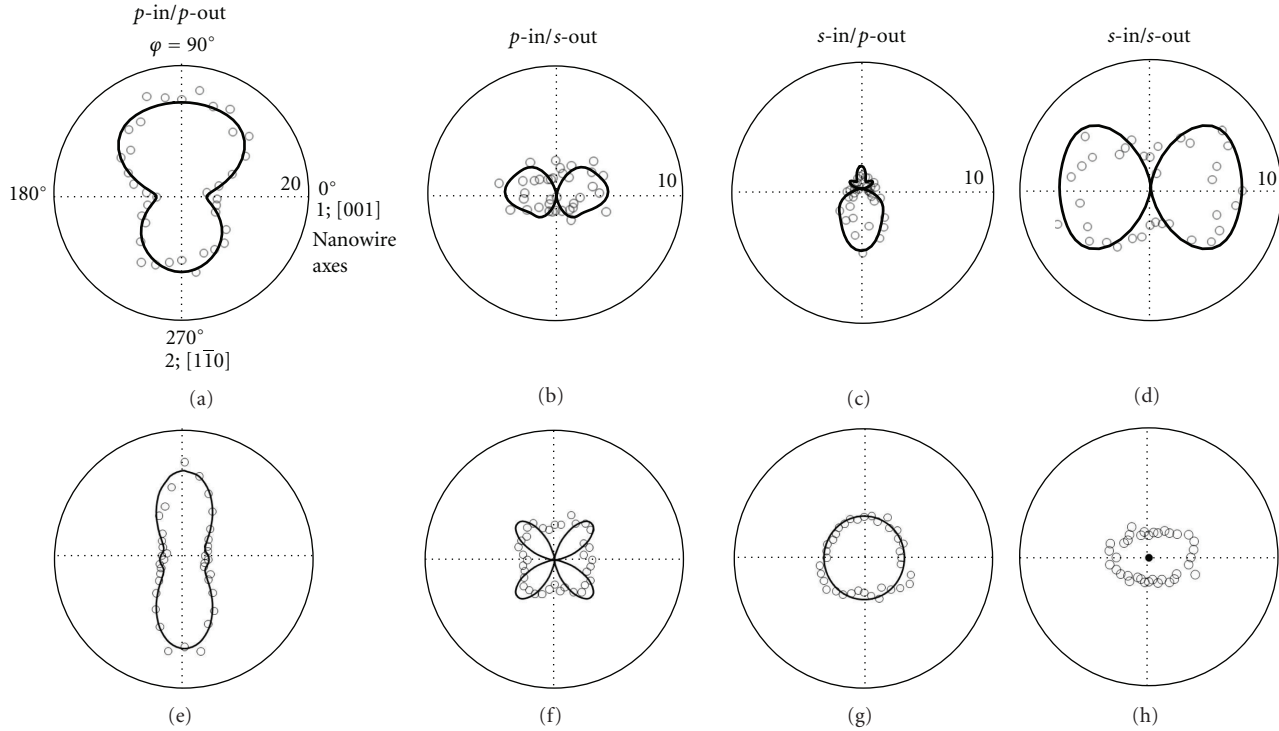*s*-in/*s*-out

(d)

(e)

(f)

(g)

(h)

FIGURE 6: SHG intensity from Pt nanowires with elliptic ((a)–(d)) and boomerang ((e)–(h)) cross-sectional shapes on the MgO(110) faceted template for $\hbar\omega = 2.33$ eV as a function of the sample rotation angle $\varphi$ for four different input and output polarization configurations indicated at the top. The sample rotation angle $\varphi$ is defined as the angle between the incident plane and the [001] (direction 1) or the nanowire axis. The solid curves are the best-fit theoretical patterns calculated with independent effective nonlinear susceptibility $\chi^{(2)}$ elements as adjustable parameters [18].

program [21]. We first calculated the SHG intensity pattern for each nonlinear optical susceptibility element by using Maxwell's equations. The SHG light at the frequency $2\omega$ is generated from this nonlinear polarization antenna as the dipole radiation following Maxwell's wave equation with the source term of nonlinear polarization.

$$\vec{\nabla} \times \left(\vec{\nabla} \times \vec{E}_{\text{SHG}}\right) + \varepsilon\mu\frac{\partial^2 \vec{E}_{\text{SHG}}}{\partial t^2} = -\mu\frac{\partial^2 \vec{P}_{2\omega}^{\text{NL}}}{\partial t^2}. \quad (1)$$

In this wave equation, the nonlinear polarization $P_i^{\text{NL}}$ on the right-hand side generates forced oscillation wave $E_{\text{SHG}}$ as a source term. The nonlinear polarization $P_i^{\text{NL}}$ induced in the nanowire array at the second harmonic frequency is written as a function of the incident electric field at $\omega$ as:

$$P_{2\omega,i}^{\text{NL}} = \varepsilon_0 \sum_{j,k=1,2,3} \chi_{ijk}^{(2)} E_j E_k. \quad (2)$$

Here, $\varepsilon_0$ is the permittivity of the free space, $\chi_{ijk}^{(2)}$ is a third-rank tensor representing the second-order nonlinear susceptibility of the nanowire array, and $E$ is the electric field of the incident light. The nonlinear susceptibility element including odd numbers of any Cartesian component in the suffix arises due to the symmetry breaking in the corresponding direction. The electric field $E$ in the nanowire array at the fundamental frequency on the right-hand side of (2)
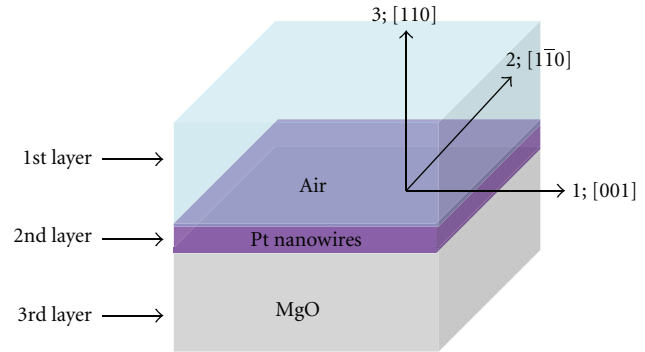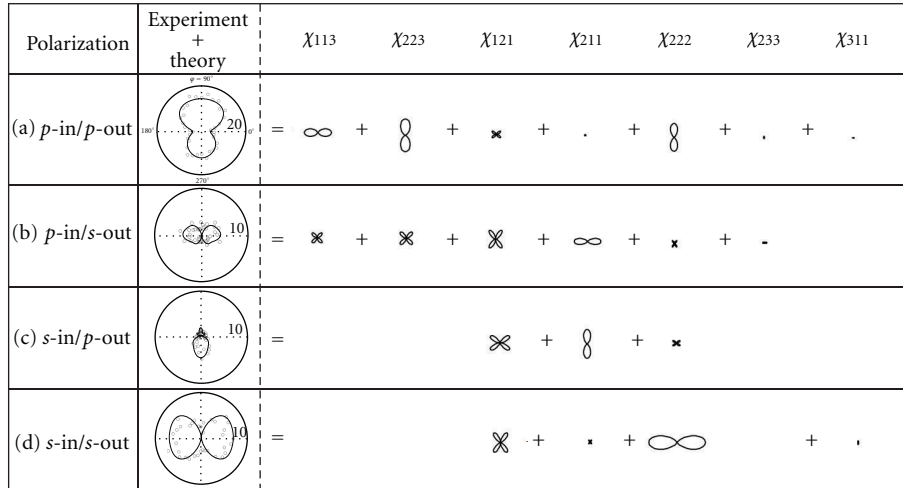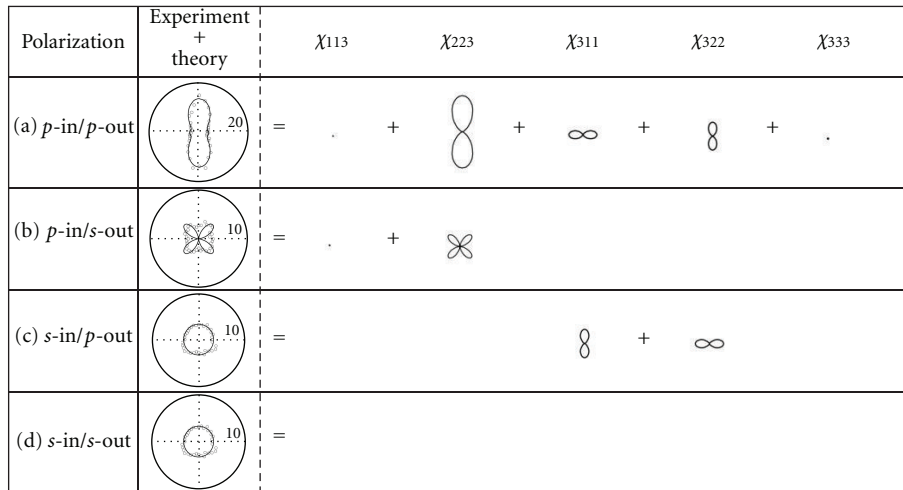


FIGURE 7: Three-layered dielectric model for calculating the SHG response from the nanowire samples; the highest layer is defined as the atmospheric region, the middle layer is a flat thin dielectric slab substituting for a nanowire array, and the lowest layer is the bulk region of MgO.

was calculated by Maxwell's equations, assuming the nanowire array as a flat thin dielectric slab as shown in Figure 7.

We fitted the theoretical SHG intensity patterns to the experimental result in Figure 6. Assuming $C_s$ symmetry of the ellipsoid Pt nanowire/MgO(110) system, there are ten independent nonlinear susceptibility elements: $\chi_{222}$, $\chi_{211}$, $\chi_{311}$, $\chi_{223}$, $\chi_{121}$, $\chi_{113}$, $\chi_{311}$, $\chi_{323}$, $\chi_{333}$ and $\chi_{322}$. Assuming $C_{2v}$ symmetry of the boomerang Pt nanowire/MgO(110) system,

| Polarization | Experiment + theory | $\chi_{113}$ | $\chi_{223}$ | $\chi_{121}$ | $\chi_{211}$ | $\chi_{222}$ | $\chi_{233}$ | $\chi_{311}$ |
|---|---|---|---|---|---|---|---|---|
| (a) $p$-in/$p$-out | | = ∞ + | ⧗ + | ✕ + | . + | ⧗ + | . + | . |
| (b) $p$-in/$s$-out | | = ✕ + | ✕ + | ✕ + | ∞ + | ✕ + | - | |
| (c) $s$-in/$p$-out | | = | | ✕ + | ⧗ + | ✕ | | |
| (d) $s$-in/$s$-out | | = | | ✕ + | . + | ∞ | + | . |

(a)

| Polarization | Experiment + theory | $\chi_{113}$ | $\chi_{223}$ | $\chi_{311}$ | $\chi_{322}$ | $\chi_{333}$ |
|---|---|---|---|---|---|---|
| (a) $p$-in/$p$-out | | = . + | ⧗ + | ∞ + | ⧗ + | . |
| (b) $p$-in/$s$-out | | = . + | ✕ | | | |
| (c) $s$-in/$p$-out | | = | | ⧗ + | ∞ | |
| (d) $s$-in/$s$-out | | = | | | | |

(b)

FIGURE 8: The calculated SHG intensity patterns decomposed into each nonlinear susceptibility element from the ones in Figure 6 for (a) $C_s$ and (b) $C_{2v}$ symmetric Pt nanowire arrays. Intensities are in arbitrary but common units in the same row.

there are five nonzero nonlinear susceptibility elements: $\chi_{113}$, $\chi_{223}$, $\chi_{311}$, $\chi_{322}$, and $\chi_{333}$. Solid curves in Figure 6 are the best-fit theoretical patterns to the experimental data (empty circles) calculated with nonlinear susceptibility $\chi^{(2)}$ elements as adjustable parameters. In Figure 8, two types of the total calculated SHG intensity are decomposed into the contributions of different nonlinear susceptibility elements. Assumptions in handling $\chi^{(2)}$ components during the fitting decomposition are described in [15, 20]. In the following we discuss the correlation between cross-sectional shapes of Pt nanowires and their nonlinear susceptibility $\chi^{(2)}$.

In Figure 8(a) the decomposition of the SHG intensity pattern from Pt nanowires with elliptic cross-section is shown. The SHG intensity pattern for the $p$-in/$p$-out polarization combination is dominated by the superposition of signals arising from the $\chi_{113}$, $\chi_{223}$, and $\chi_{222}$ elements. The elements of $\chi_{113}$ and $\chi_{223}$ originate from the broken symmetry in direction 3, and $\chi_{222}$ originates from the broken symmetry in direction 2. The total SHG intensity pattern is asymmetric

in the vertical direction due to the interference between the contribution of $\chi_{223}$ and $\chi_{222}$ susceptibility elements. Thus we can say that the pattern for this polarization combination should be sensitive to the shape of the cross-section of the nanowires.

Next, we see the SHG intensity pattern in the $s$-in/$s$-out polarization configuration. The SHG intensity pattern has two clear lobes at $\varphi = 0°$ and $180°$. As we pointed out in our previous work [15], the broken symmetry is considered to occur at the asymmetric part indicated by an arrow in Figure 9. In Figure 8(a) we see that the contribution of $\chi_{222}$ is the biggest among those of all the susceptibility elements. We can say that the SHG intensity at $\varphi = 0°$ and $180°$ solely reflects the contribution of $\chi_{222}$ and hence of the broken symmetry in direction 2. In Figure 9 the edge structure surrounded by the dashed ellipse has a size of 1 to 2 nm. The motion of electrons in this structure is remarkably restricted, and a second-order nonlinear optical effect occurs. In fact in another previous work by us we observed relatively strong
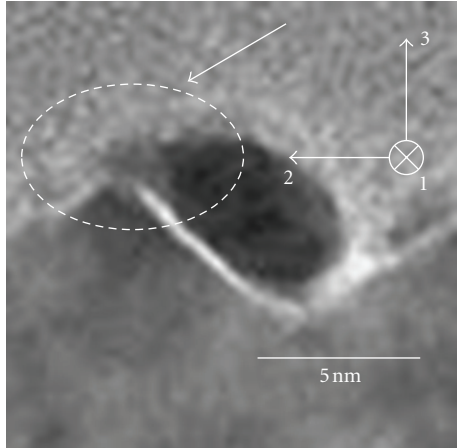
FIGURE 9: The expanded TEM image of a Pt nanowire on a MgO(110) faceted template. The area indicated by an arrow is asymmetric especially in direction 2.

SHG from Pt nanowires with 2 nm widths [19]. These facts are consistent with each other. As a constraint of the electron movement, a quantum confinement effect is the most plausible candidate.

When there is a symmetry breaking in direction 2 (or 3), the nonzero nonlinear susceptibility element has odd number of 2's (or 3's) in the suffices. In the present case there are four nonlinear susceptibility elements $\chi_{121}$, $\chi_{211}$, $\chi_{222}$, and $\chi_{233}$ due to the broken symmetry in direction 2. We also have three nonlinear susceptibility elements $\chi_{311}$, $\chi_{113}$, and $\chi_{223}$ arising from the broken symmetry in direction 3.

In Figure 8(b) the total calculated SHG intensity from boomerang nanowires is decomposed into contributions of different nonlinear susceptibility elements. In Figure 8(b) the contribution of the nonlinear susceptibility elements has a relation as $|\chi_{223}| \gg |\chi_{113}|$, and $\chi_{223}$ dominates the SHG intensity pattern shape in the $p$-in/$p$-out polarization configuration. This relation is consistent with the fact that the nanowires have a boomerang cross-section in the 2-3 plane. This cross-sectional shape makes the motion of electrons in the mix of directions 2 and 3 with each other and makes the observed optical nonlinearity. On the other hand, the nanowire has a translational symmetry in the direction 1 and the optical nonlinearity $\chi_{113}$ is not large.

The nonlinear optical susceptibility element $\chi_{223}$ should also make the fourfold symmetric SHG intensity pattern in $p$-in/$s$-out polarization configuration as seen in Figure 8(b), although the calculation does not reproduce the experiment completely as seen in Figure 6(f). In Figure 8(b) we find that the contributions of the nonlinear susceptibility of $\chi_{322}$ and $\chi_{311}$ are of the same magnitude. As a result, the contributions of the $\chi_{223}$, $\chi_{311}$, and $\chi_{322}$ elements are proved to be dominant in the $p$-in/$p$-out, $p$-in/$s$-out, and $s$-in/$p$-out polarization configurations. These nonlinear susceptibility elements occur due to the broken symmetry in direction 3.

On the other hand, the theoretical SHG intensity pattern with $C_{2v}$ symmetry did not reproduce the experimental data in $s$-in/$s$-out polarization configuration. This nonzero response of the signal in the $s$-in/$s$-out polarization combination is suggested to be due to the roughness as discussed below.

Here we comment on the contribution of the quadrupolar effect in our SHG signals. The SHG intensity from a MgO bulk crystal was at the noise level as we found out in a separate experiment. Thus we can say that the electronic quadruple effect from the MgO bulk can be disregarded. On the contrary, the SHG from nanowires with several nm thickness generally includes both dipole and electronic quadruple effects. Dipolar SHG originating from the third-rank tensor is sensitive to the asymmetry of the structure, while quadrupolar SHG originating from the fourth-rank tensor is insensitive to it. In Figure 6 the angular SHG patterns observed from two kinds of nanowires show sensitive dependence on the asymmetry of the nanowire cross-sections. Therefore, it is suggested that the quadrupolar effect is not dominant.

*3.3. Roughness Effect.* For the boomerang nanowires we intended to remove the asymmetry of the platinum shape in direction 2 at the tops of the MgO facets by depositing the platinum from two directions. Thus the nonlinear susceptibility element $\chi_{222}$ was expected to be cancelled. In Figure 8(b) with the assumption of $C_{2v}$, all the susceptibility elements have vanishing contribution to the SHG intensity pattern in the $s$-in/$s$-out polarization configuration. Contrary to this expectation, we see nonzero SHG intensity for the $s$-in/$s$-out combination with peaks at $\varphi = 0°$ and $180°$ as seen in Figure 6(h).

As the candidate origin of this remaining SHG intensity in the $s$-in/$s$-out polarization configuration, the imperfections of the shapes of the nanowires are suggested. Naturally, there are geometrical imperfections in the structures of fabricated Pt nanowires as we can see in Figures 4(a) and 4(b). We see more remarkable imperfections for the boomerang cross-sectioned nanowires in Figure 4(b) than for the elliptic cross-sectioned nanowires in Figure 4(a). In Figure 4(c) we see the width distribution in the two types of nanowires, and we see here also that the boomerang nanowires have broader width distribution.

A closer look at the cross-sectional TEM images of the macroscopic $C_{2v}$ sample showed there are asymmetric boomerangs like those shown schematically in Figure 10. Approximately 30% of the nanowire cross-sections examined had such asymmetric boomerang cross-sections. Then nonlinear polarizations $P_2^{NL}$ induced by the incident electric field in direction 2 at the cross-sections like those in Figure 10 should have opposite signs to each other. Statistically, the reflected SHG light-from these two kinds of structures should cancel each other if we assume a random distribution. However, the fact that SHG is observed in Figure 6(h) indicates that the cancellation of the SHG from the two types of the asymmetric nanowires was incomplete.

As one of the candidate, we can think of the effect of platinum nanodots on the SHG intensity patterns. Kitahara et al. reported isotropic SHG in the $p$-in/$p$-out and $s$-in/$p$-out polarization configurations from Au nanodots on the NaCl(110) faceted templates [12]. Therefore, there can be
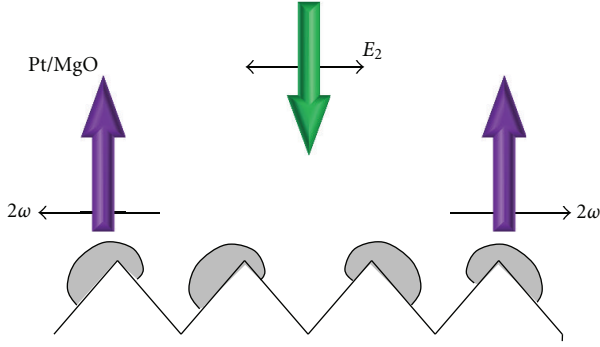
FIGURE 10: The model of cancellation of the SHG signal from two types of asymmetric nanowires. The nonlinear polarizations $P_2^{\mathrm{NL}}$ induced by the incident electric field in direction 2 have opposite signs due to the asymmetric shapes. The reflected SHG lights should be cancelled by each other when the nanowires have random distribution.

contribution of the Pt nanodots in the $p$-in/$p$-out and $s$-in/$p$-out polarization configurations in Figures 6(e) and 6(g), but not in the $s$-in/$s$-out polarization configuration.

As another candidate we consider the polarization scrambling of the light field, induced by the roughness of the nanowire structures seen in Figure 4(b). We consider the conversion of the $s$-polarized incident field of frequency $\omega$ by the roughness $\zeta(x, y)$ [22] of the metal nanowire structure. Here, $\zeta(x, y)$ represents the deviation of the height of the metal surface of the nanowires from that of the ideal ones. We consider the case of $\varphi = 0°$ so that the wave vector component of the incident light parallel to the substrate is in direction 1. The electric field of the $s$-polarized incident light is in direction 2. The electric field $\vec{E}_{\mathrm{NF}}^{\omega}$ near the nanowire is expanded generally with respect to $\zeta(x, y)$ as

$$\vec{E}_{\mathrm{NF}} = E_2 \vec{e}_2 + \varsigma(x, y)\left(c_{21}^{(1)}\vec{e}_1 + c_{23}^{(1)}\vec{e}_3\right)E_2$$
$$+ \varsigma(x, y)^2\left(c_{21}^{(2)}\vec{e}_1 + c_{23}^{(2)}\vec{e}_3\right)E_2. \tag{3}$$

Here, $C_{jk}^{(i)}$ is a coefficient describing the rate of the conversion of the $j$-polarized electric field into $k$-polarized one. $\vec{e}_1$ and $\vec{e}_3$ are unit vectors in the directions 1 and 3, respectively. Averaging (2) over the area on the substrate of a wavelength size, the second term vanishes and (2) becomes

$$\left\langle \vec{E}_{\mathrm{NF}} \right\rangle = E_2 \vec{e}_2 + \left\langle \varsigma \right\rangle\left(c_{21}^{(1)}\vec{e}_1 + c_{23}^{(1)}\vec{e}_3\right)E_2$$
$$+ \left\langle \varsigma^2 \right\rangle\left(c_{21}^{(2)}\vec{e}_1 + c_{23}^{(2)}\vec{e}_3\right)E_2 \tag{4}$$
$$= E_2 \vec{e}_2 + \left\langle \varsigma^2 \right\rangle\left(c_{21}^{(2)}\vec{e}_1 + c_{23}^{(2)}\vec{e}_3\right)E_2$$

since $\langle \zeta \rangle = 0$. Hence, the 3rd component of the averaged electric field is

$$\langle E_{\mathrm{NF3}} \rangle = \langle \varsigma^2 \rangle c_{23}^{(2)} E_2. \tag{5}$$

On the other hand, the contribution of the nonlinear optical susceptibility element $\chi_{223}^{(2)}$ was dominantly responsible for
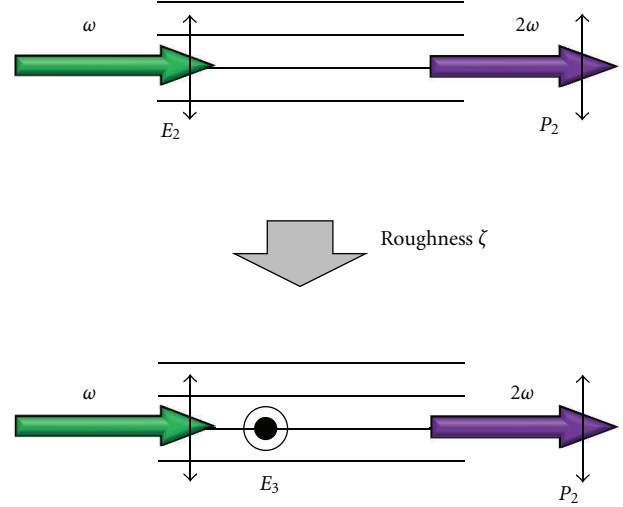


FIGURE 11: The polarization scrambling effect induced by the structural roughness of nanowires. The electric field component $E_3$ is newly induced by the roughness $\zeta$ in the lower panel.

the enhancement of the SHG intensity at $\varphi = 90°$ and $270°$ in the $p$-in/$p$-out polarization configuration as seen in Figure 6(a). This nonlinear susceptibility element gives a nonlinear polarization:

$$P_2^{\mathrm{NL}} = \varepsilon_0 \chi_{223}^{(2)} E_2^{\omega} E_3^{\omega}. \tag{6}$$

Substituting the 3rd component of (5) for $E_3^{\omega}$ in (6), we obtain

$$P_2^{\mathrm{NL}} = \varepsilon_0 \chi_{223}^{(2)} E_2^{\omega} \left\langle E_{\mathrm{NF3}}^{\omega} \right\rangle$$
$$= \varepsilon_0 \chi_{223}^{(2)} E_2^{\omega} \left\langle \zeta^2 \right\rangle c_{23}^{(2)} E_2^{\omega}. \tag{7}$$

Equation (7) indicates that the roughness on the nanowires generates SHG in $s$-in/$s$-out polarization configuration at $\varphi = 0°$. If $\langle E_{\mathrm{NF3}}^{\omega} \rangle$ depends weakly on the direction of the incident electric field, the SHG intensity generated by (7) in $s$-in/$s$-out should be as:

$$I_{s\text{-in}/s\text{-out}}^{2\omega} \propto \left| \chi_{20}^{(2)} E_{20}^{\omega} \cos^2\varphi \right|^2. \tag{8}$$

Equation (8) is large when the incident electric field is in direction 2. In this configuration, $\varphi$ is $0°$ or $180°$. This is consistent with the pattern observed in Figure 6(h).

Namely, induced by the roughness, the $s$-polarized incident light contains a finite local electric field component $E_3$ in the direction normal to the wire array face as shown in Figure 11. For our nanowires the $\chi_{223}^{(2)}$ component has been confirmed to be dominant as we have already seen in Figure 8(b). Therefore, the nonlinear polarization $P_2^{\mathrm{NL}}$ is generated by the fundamental electric field $E_2$ and the roughness-induced $E_3$ components. The SHG intensity pattern in Figure 6(h) has peaks rotated by $90°$ from those in Figure 6(e), since the incident and SHG electric fields are rotated by $90°$ from each other between $p$- and $s$-polarizations.

The discrepancy between the experimental SHG data and theoretical pattern seen in Figure 6(f) at $\varphi = 0°$, 90°, 180°, and 270° may also be ascribed to the imperfections of the nanowire structures. Namely, in the inset of Figure 4(b) we see slight local undulation of the Pt nanowires in the several-nanometer scale. This undulation of the nanowires should add isotropic SHG component to the pattern. Namely, the undulation compromises the directionality of the nanowire axes and disturbs the SHG intensity pattern in Figure 6(f).

The effect of the roughness here could also be described by the second-order roughness perturbation. However, we were not successful in explaining the isotropic component in Figure 6(f) with this treatment. Hence, a quantitative analysis of this pattern change will require more detailed models.

## 4. Conclusion

We have obtained the Pt nanowires with elliptic and boomerang-like cross-sections on the MgO(110) faceted template. From their SHG intensity patterns, the nonlinear susceptibility elements corresponding to the $C_s$ and $C_{2v}$ symmetry of the nanowire structure were identified, respectively. We have concluded that the control of the nanowires cross-sections has led to the change in their nonlinear optical property. For the nanowires with $C_s$ symmetry and the elliptic cross-sections, the contribution of the nonlinear optical susceptibility element $\chi_{222}$ due to the broken symmetry in direction 2 was responsible for the enhancement of the SHG intensity at $\varphi = 0°$ and 180° in the $s$-in/$s$-out polarization configuration. For the nanowires with $C_{2v}$ symmetry and the boomerang cross-sections, the nonlinear susceptibility elements $\chi_{113}$, $\chi_{223}$, $\chi_{311}$, and $\chi_{322}$ due to the broken symmetry in direction 3 dominate the SHG response in the $p$-in/$p$-out, $p$-in/$s$-out, and $s$-in/$p$-out polarization configurations. The SHG signals observed in the $s$-in/$s$-out polarization configuration are suggested to originate from the imperfections of the nanowire structure.

## References

[1] S. W. Liu, H. J. Zhou, A. Ricca, R. Tian, and M. Xiao, "Far-field second-harmonic fingerprint of twinning in single ZnO rods," *Physical Review B*, vol. 77, no. 11, Article ID 113311, 4 pages, 2008.

[2] H. M. Su, J. T. Ye, Z. K. Tang, and K. S. Wong, "Resonant second-harmonic generation in monosized and aligned single-walled carbon nanotubes," *Physical Review B*, vol. 77, no. 12, Article ID 125428, 4 pages, 2008.

[3] F. Dutto, C. Raillon, K. Schenk, and A. Radenovic, "Nonlinear optical response in single alkaline niobate nanowires," *Nano Letters*, vol. 11, no. 6, pp. 2517–2521, 2011.

[4] A. Zangwill, *Physics at Surfaces*, Cambridge University Press, New York, NY, USA, 1988.

[5] J. C. Johnson, H. Yan, R. D. Schaller, P. B. Petersen, P. Yang, and R. J. Saykally, "Near-field imaging of nonlinear optical mixing in single zinc oxide nanowires," *Nano Letters*, vol. 2, no. 4, pp. 279–283, 2002.

[6] G. Schider, J. R. Krenn, W. Gotschy et al., "Optical properties of Ag and Au nanowire gratings," *Journal of Applied Physics*, vol. 90, no. 8, pp. 3825–3830, 2001.

[7] V. Barzda, R. Cisek, T. L. Spencer, U. Philipose, H. E. Ruda, and A. Shik, "Giant anisotropy of second harmonic generation for a single ZnSe nanowire," *Applied Physics Letters*, vol. 92, no. 11, Article ID 113111, 3 pages, 2008.

[8] A. Lesuffleur, P. Gogol, P. Beauvillain, B. Guizal, D. Van Labeke, and P. Georges, "Nonlinear optical properties of interconnected gold nanoparticles on silicon," *Journal of Applied Physics*, vol. 104, no. 12, Article ID 124310, 4 pages, 2008.

[9] I. V. Kityk, J. Ebothé, I. Fuks-Janczarek et al., "Nonlinear optical properties of Au nanoparticles on indium-tin oxide substrate," *Nanotechnology*, vol. 16, no. 9, pp. 1687–1692, 2005.

[10] J. Ebothe, I. V. Kityk, G. Chang, M. Oyama, and K. J. Plucinski, "Pd nanoparticles as new materials for acoustically induced non-linear optics," *Physica E*, vol. 35, no. 1, pp. 121–125, 2006.

[11] C. G. Biris and N. C. Panoiu, "Second harmonic generation in metamaterials based on homogeneous centrosymmetric nanowires," *Physical Review B*, vol. 81, no. 19, Article ID 195102, 16 pages, 2010.

[12] T. Kitahara, A. Sugawara, H. Sano, and G. Mizutani, "Anisotropic optical second-harmonic generation from the Au nanowire array on the NaCl(1 1 0) template," *Applied Surface Science*, vol. 219, no. 3-4, pp. 271–275, 2003.

[13] N. Hayashi, K. Aratake, R. Okushio et al., "Optical second harmonic generation from Pt nanowires," *Applied Surface Science*, vol. 253, no. 22, pp. 8933–8938, 2007.

[14] Y. Ogata, N. A. Tuan, S. Takase, and G. Mizutani, "Polarization and azimuthal angle dependence of the optical second harmonic generation from Pt nanowires on the MgO(110) faceted template," *Surface and Interface Analysis*, vol. 42, no. 10-11, pp. 1663–1666, 2010.

[15] Y. Ogata, N. A. Tuan, and G. Mizutani, "Analysis of the optical second harmonic generation from Pt nanowires on the faceted MgO(110) template," *Journal of Surface Analysis*, vol. 17, no. 3, pp. 252–255, 2011.

[16] T. Shinjo and T. Ono, "Magnetoresistance of multilayers on microstructured substrates," *Journal of Magnetism and Magnetic Materials*, vol. 156, no. 1–3, pp. 11–14, 1996.

[17] A. Sugawara and K. Mae, "Faceting of homoepitaxial MgO(1 1 0) layers prepared by electron beam evaporation," *Surface Science*, vol. 558, no. 1–3, pp. 211–217, 2004.

[18] A. Sugawara, T. Coyle, G. G. Hembree, and M. R. Scheinfein, "Self-organized Fe nanowire arrays prepared by shadow deposition on NaCl(110) templates," *Applied Physics Letters*, vol. 70, no. 8, pp. 1043–1045, 1997.

[19] Y. Ogata, Y. Iwase, Y. Miyauchi, and G. Mizutani, "Optical second harmonic generation from the array of 2 nm-width Pt nanowires on the MgO(210) faceted template," in *Proceedings of the 11th IEEE International Conference on Nanotechnology*, pp. 1661–1664, 2011.

[20] Y. Ogata, N. Anh Tuan, Y. Miyauchi, and G. Mizutani, "Optical second harmonic generation from Pt nanowires with boomerang-like cross-sectional shapes," *Journal of Applied Physics*, vol. 110, no. 4, Article ID 044301, 6 pages, 2011.

[21] E. Kobayashi, G. Mizutani, and S. Ushioda, "Surface optical second harmonic generation from rutile $TiO_2(110)$ in air," *Japanese Journal of Applied Physics, Part 1*, vol. 36, no. 12, pp. 7250–7256, 1997.

[22] A. A. Maradudin and D. L. Mills, "Scattering and absorption of electromagnetic radiation by a semi-infinite medium in the presence of surface roughness," *Physical Review B*, vol. 11, no. 4, pp. 1392–1415, 1975.